Different molecular bases underlie the mitochondrial respiratory activity in the homoeothermic spadices of *Symplocarpus renifolius* and the transiently thermogenic appendices of *Arum maculatum*

Yusuke KAKIZAKI*, Anthony L. MOORE† and Kikukatsu ITO‡[1]

*The United Graduate School of Agricultural Sciences, Iwate University, 3-18-8 Ueda, Morioka, Iwate, 020-8550, Japan, †Department of Biochemistry and Molecular Biology, School of Life Sciences, University of Sussex, Falmer, Brighton, BN1 9QG, U.K., and ‡Cryobiofrontier Research Center, Faculty of Agriculture, Iwate University, 3-18-8 Ueda, Morioka, Iwate, 020-8550, Japan

Symplocarpus renifolius and *Arum maculatum* are known to produce significant heat during the course of their floral development, but they use different regulatory mechanisms, i.e. homoeothermic compared with transient thermogenesis. To further clarify the molecular basis of species-specific thermogenesis in plants, in the present study we have analysed the native structures and expression patterns of the mitochondrial respiratory components in *S. renifolius* and *A. maculatum*. Our comparative analysis using Blue native PAGE combined with nano LC (liquid chromatography)-MS/MS (tandem MS) has revealed that the constituents of the respiratory complexes in both plants were basically similar, but that several mitochondrial components appeared to be differently expressed in their thermogenic organs. Namely, complex II in *S. renifolius* was

detected as a 340 kDa product, suggesting an oligomeric or supramolecular structure *in vivo*. Moreover, the expression of an external NAD(P)H dehydrogenase was found to be higher in *A. maculatum* than in *S. renifolius*, whereas an internal NAD(P)H dehydrogenase was expressed at a similar level in both species. Alternative oxidase was detected as smear-like signals that were elongated on the first dimension with a peak at around 200 kDa in both species. The significance and implication of these data are discussed in terms of thermoregulation in plants.

Key words: alternative oxidase (AOX), Blue native PAGE, mitochondrial respiratory chain, thermogenic plants, type II NAD(P)H dehydrogenase.

INTRODUCTION

Organ-specific thermogenesis associated with floral development has been well documented in plants from a diverse range of families, including the monocotyledonous *Araceae* [1], dicotyledonous *Nelumbonaceae* [2] and gymnospermous *Cycadaceae* [3]. Most thermogenic activities in these plants can be categorized into two types, in accordance with the transition patterns of their tissue temperature. Transient heat production has been observed in the majority of thermogenic plants analysed, where the temperature of a thermogenic organ rises discontinuously over one or two events. This type of thermogenesis has been well studied in *Arum* species since Jean-Baptiste Lamarck first documented the thermogenic activity of plants in the European arum lily [4]. For instance, it is now widely known that appendices of *Arum maculatum* can be hotter than 30°C at the peak of their transient thermogenesis, when the ambient temperature is between 7–22°C [5,6,7]. On the other hand, homoeothermic heat production has also been reported in a limited number of species, such as sacred lotus (*Nelumbo nucifera*) and skunk cabbage (*Symplocarpus* species) [2,8,9]. In these plants, the thermogenic organ remains at a constant temperature for several days with remarkable precision. For example, the spadices of *S. renifolius* are reported to maintain their tissue temperature at a relatively stable $21 \pm 2.4°C$, although the ambient temperature varies over a wide range [8]. Surprisingly, this plant can produce heat that is sufficient to melt the surrounding snow in its natural environment [10].

The molecular basis of thermogenesis in plants has long been associated with the expression of cyanide-resistant respiration [4]. Such respiration is attributed to the activity of AOX (alternative oxidase), which is located on the matrix surface of the inner mitochondrial membrane and catalyses the oxidation of ubiquinol and the reduction of molecular oxygen to water [11]. AOX is an energy-dissipative enzyme, since it does not contribute to the formation of a proton electrochemical gradient across the inner membrane and, as a consequence, to ATP synthesis. The drastic change in free energy which is accompanied by the reaction catalysed by AOX is believed to be liberated as heat in thermogenic plants. In fact, a large cyanide-resistant respiration capacity has been observed to be associated with thermogenesis in plants, regardless of whether it is transient or homoeothermic [12,13]. Although a large quantity of AOX protein has been shown to accumulate in mitochondria following the onset of thermogenesis in some species [13,14], this is not the prerequisite for a considerable cyanide-resistant respiration capacity as previously demonstrated in *A. maculatum* [12].

BN-PAGE (Blue native PAGE) has become a major technique in the analysis of multiprotein complexes, particularly those localized to membranes [15]. This method is especially effective when combined with 2D (two-dimensional) SDS/PAGE and MS, as it is then possible to identify the constitutive subunits of a complex. All of the typical plant mitochondrial respiratory complexes have been characterized using this technique [16,17], the major findings of which have revealed that there are distinct differences between plant and mammalian mitochondria, such

as an eight-subunit complex II and also plant-specific subunits that are associated with complex IV [18]. A number of the supramolecular structures of the respiratory complexes, i.e. supercomplexes, have also been successfully characterized using BN-PAGE in plants. Supercomplex $I+III_2$ is highly abundant in a number of species [16], whereas the expressions of other supercomplexes, such as I_2+III_4 and $I+III_2+IVa_4$, which are generally at low abundance, vary even between organs of the same species [17].

Previously, the structures of the respiratory complexes in mitochondria from thermogenic appendices of *A. maculatum* were also analysed using BN-PAGE, but few striking characteristics that are unique to thermogenic species were detected [19]. In view of the finding that that study only focused on *A. maculatum*, but did not consider homoeothermic plants, which appear to precisely regulate their metabolic flux, it is conceivable that such tissues may possess different respiratory characteristics in comparison with *A. maculatum*. Furthermore, although AOX has been analysed in previous studies, scant attention has been paid to other non-oxidative phosphorylation components, such as the type II NAD(P)H dehydrogenases. In light of the above, further investigations into the characteristics of the respiratory chain of thermogenic plants seems warranted.

In the present study, we have analysed the expression profile and native structures of the respiratory components of mitochondria from the stigma-stage spadix of *S. renifolius*, a homoeothermic organ, in addition to the δ-stage appendix of *A. maculatum*, a transiently thermogenic organ. Our primary objective was to examine whether mitochondria of these plants have different molecular mechanisms underlying their respective thermogenic activities. To this end, not only the respiratory components, but also an extensive range of mitochondrial proteins, were subjected to qualitative comparative analyses between these two species. We reveal two notable differences in the respiratory chains of these plants; namely an irregularly large sized complex II is present in *S. renifolius*, but not in *A. maculatum*, and a type II NAD(P)H dehydrogenase appears to be expressed at a much higher level in *A. maculatum* than in *S. renifolius*. Furthermore, our results suggest that the respiratory pathways which normally function during thermogenesis are different in the two thermogenic plants.

EXPERIMENTAL

Plant materials

For the preparation of mitochondria, spadices of *S. renifolius* were collected from their natural environments in Hakuba, Nagano prefecture, Japan, in April 2008, as well as in Omori, Akita prefecture, Japan, in April 2010. Appendices of *A. maculatum* were collected from the campus of the University of Sussex, Brighton, U.K., in May 2010. The thermogenic stages of the plants were classified according to the morphological changes in their inflorescences as described previously [5,9,20]. For the preparation of RNA, tissue samples of *S. renifolius* were collected in Daisen, Akita prefecture, Japan, in March 2007, and in Fujine, Iwate prefecture, Japan, in March 2012, and those of *A. maculatum* were collected on the campus of the University of Sussex in May 2009. These samples were flash-frozen in liquid nitrogen to prevent RNA degradation.

Isolation of mitochondria

Mitochondria from *S. renifolius* spadices and *A. maculatum* appendices were isolated as described previously [21,22];

however, 27%–45%–60% Percoll gradients were used for both *S. renifolius* and *A. maculatum*. Mitochondria from *Schizosaccharomyces pombe* Sp.011 were isolated according to an established protocol [23]. The isolated mitochondria were stored at $-80\,^{\circ}$C and were aliquoted on the first thawing.

Protein concentration determination

Protein concentrations of isolated mitochondria were determined by the BCA (bicinchoninic acid) method using a BCA Protein Assay Kit (Pierce). Various concentrations of BSA in the range of 0–2000 μg/ml were used as the reference standards.

1D (one-dimensional) BN-PAGE and 2D BN/SDS/PAGE

Mitochondrial proteins were solubilized in digitonin using a NativePAGE Sample Prep Kit (Invitrogen) as instructed by the manufacturer. The 1D BN-PAGE was performed using NativePAGE Novex 4–16% Bis-Tris Gels (Invitrogen) and an XCell SureLock Mini-Cell (Invitrogen). Approximately 50 μg of the solubilized proteins was loaded per lane and electrophoresed for 150 min at 150 V with NativeMark Unstained Protein Standards (Invitrogen). After 50 min of electrophoresis, 'dark cathode buffer' (Invitrogen) containing 0.02% Coomassie Brilliant Blue G-250 was substituted with 'light cathode buffer' (Invitrogen) containing 0.002% Coomassie Brilliant Blue G-250. For 2D BN/SDS/PAGE, a gel strip underwent reductive alkylation as instructed by the manufacturer and was then loaded on to NuPAGE Novex 4–12% Bis-Tris ZOOM Gels (Invitrogen). The electrophoresis was performed in NuPAGE Mops SDS Running Buffer (Invitrogen) for 55 min at 200 V. PageRuler Prestained Protein Ladder (Fermentas) or Precision Plus Protein Dual Color Standards (Bio-Rad Laboratories) was used as the protein standards for the 2D BN/SDS/PAGE. Visualization of the proteins was achieved by incubating the gels in Quick-CBB PLUS (Wako Pure Chemical Industries).

Mass spectrometry

Protein spots visualized on a 2D BN/SDS/PAGE gel were excised with sterile knives and were subjected to in-gel digestion with Sequencing Grade Modified Trypsin (Promega). The resulting peptides were purified using Zip Tip pipette tips (Millipore) and were eluted in 15 μl of 0.1% TFA (trifluoroacetic acid). The peptide solutions were then separated using an Advance UHPLC (ultra-high performance liquid chromatography) system (Michrom Bioresources) connected to an L-column Micro 0.3 mm×5 mm (CERI) as the trap column and a Magic C18 AQ nano column 0.1 mm×150 mm (Michrom Bioresources) as the separation column. The retained peptides were eluted using a linear gradient of acetonitrile from 5% to 45% (v/v) at a flow rate of 500 nl/min and were subsequently ionized with an Advance spray source (Michrom Bioresources) at 1.8 kV. Mass spectrometric analyses of the peptides were carried out using an LTQ Orbitrap XL (Thermo Fisher Scientific) operated by Xcalibur software version 2.0.7 (Thermo Fisher Scientific). The raw MS/MS (tandem MS) spectra files were first converted into mgf (Mascot generic format) files using Proteome Discoverer (Thermo Fisher Scientific) and were subsequently processed by MASCOT search version 2.3.02 (Matrix Science) with the following parameters: database, NCBInr + contaminants (compiled by the Max-Planck Institute of Biochemistry, Martinsried, Germany); arrow up to 1 missed cleavage; taxonomy, viridiplantae; variable modifications, oxidation of methionine; peptide mass tolerance, 10 p.p.m.; MS/MS tolerance, 0.2 kDa; peptide charge, 2^+ and 3^+;

significance threshold, $P < 0.05$; and cut-off expectation value, 0.05.

Western blotting and immunological detection

Proteins separated by either 1D BN-PAGE or 2D BN/SDS/PAGE were transferred to an Immobilon P membrane (Millipore) at 45 V and 1 mA per cm^2 for 90 min. In the case of Western blotting following 1D BN-PAGE, the membrane was sequentially incubated in 8 % acetate for 15 min and then in deionized water for 5 min to be dried; this drying procedure was indispensable for clear immunological detection because methanol incubation during the rehydration process eliminates undesirable Coomassie Brilliant Blue G-250 from the membrane. The membrane was then treated as described previously [21] with the addition of an overnight incubation with AOA monoclonal antibody (Agrisera) at 4 °C.

Isolation of *NDA*, *NDB* and *EF1α* cDNAs

Total RNAs were extracted from thermogenic organs, i.e. a stigma-stage spadix of *S. renifolius* and a $\gamma-\delta$-stage appendix of *A. maculatum*, using either an RNeasy Plant mini kit (Qiagen) or a FastPure RNA kit (Takara Bio). First strand cDNAs were generated using a PrimeScript II 1st strand cDNA Synthesis kit (Takara Bio) and an oligo dT primer. Partial fragments of the targeted transcripts were first amplified by PCR using the following primers (for all primer sequences, see Supplementary Table S1 at http://www.BiochemJ.org/bj/445/bj4450237add.htm): NDAF1-NDAR1, NDAF2-NDAR2 and NDAF3-NDAR3 for fragments from *NDA*; NDBF1-NDBR1, NDBF2-NDBR2 and NDBF3-NDBR3 followed by NDBF4-NDBR4 for fragments from *NDB*; and EF1aF1-EF1aR1 for fragments from *EF1α*. Gene-specific primers were then prepared to perform 5′- and 3′-RACE (rapid amplification of cDNA ends) with the SMARTer RACE cDNA Amplification kit (Clontech). The primers were used as follows: SrNDAR1 (where Sr is *S. renifolius*) for 5′-RACE of *SrNDA*; SrNDAF1 for 3′-RACE of *SrNDA*; SrNDBR1 and SrNDBR2 for 5′-RACE of *SrNDB*; SrNDBF1 and SrNDBF2 for 3′-RACE of *SrNDB*; AmSrEF1aR1 (where Am is *A. maculatum*) and AmSrEF1aR2 for 5′-RACE of *SrEF1α*; AmSrEF1aF1 for 3′-RACE of *SrEF1α*; AmNDAR1 for 5′-RACE of *AmNDA*; AmNDAF1 for 3′-RACE of *AmNDA*; AmNDBR1 for 5′-RACE of *AmNDB*; AmNDBF1 for 3′-RACE of *AmNDB*; AmSrEF1aR1 and AmSrEF1aR2 for 5′-RACE of *AmEF1α*; and AmSrEF1aF1 for 3′-RACE of *AmEF1α*. To isolate the full-length cDNAs, final PCR amplifications were performed with KOD-Plus (Toyobo) using the following gene-specific primers: SrNDAF2-SrNDAR2 for *SrNDA1* (DDBJ accession number: AB677831) and *SrNDA2* (AB677832); SrNDBF3-SrNDBR3 for *SrNDB1* (AB677833) and *SrNDB2* (AB677834); SrEF1aF1-SrEF1aR1 for *SrEF1α1* (AB677835); AmNDAF2-AmNDAR2 followed by AmNDAF3-AmNDAR3 for *AmNDA1* (AB677836); AmNDBF2-AmNDBR2 for *AmNDB1* (AB677837), and AmEF1aF1-AmEF1aR1 for *AmEF1α1* (AB677838). The obtained fragments were then cloned into pCR2.1 (Invitrogen) and sequenced in both directions. The large $(AG)_n$ region and its proximity in the 5′-UTR (untranslated region) of *AmNDB1* in some cases enabled it to be sequenced from one direction only. Each full-length sequence was determined by isolating two clones carrying identical inserts. However, slight differences in the number of simple sequence repeats such as $(AG)_n$ and $(CT)_n$ within the UTR were allowed for. DNA sequences were analysed using GENETYX (Genetyx).

Phylogenetic analysis of NDA and NDB

The phylogeny of the type II NAD(P)H dehydrogenases from *S. renifolius* and *A. maculatum* was analysed using MEGA4 [24] at the protein level. An alignment was generated using a ClustalW algorithm with the following sequences (GenBank® accession numbers in parentheses): *Arabidopsis thaliana* NDA1 (NP_563783), AtNDA2 (NP_180560); *Oryza sativa* NDA (NP_001044694), OsNDA (NP_001060003); *Populus trichocarpa* NDA (XP_002305005), PtNDA (XP_002313376), PtNDA (XP_002317236); *Ricinus communis* NDA (XP_002521423), RcNDA (XP_002525658); *Sorghum bicolor* NDA (XP_002456580), SbNDA (XP_002460866); *Solanum tuberosum* NDA (CAB52796); *Vitis vinifera* NDA (XP_002262771), VvNDA (XP_002277505); *Zea mays* NDA (NP_001168889); SrNDA1; SrNDA2; AmNDA1; AtNDB1 (NP_567801); AtNDB2 (NP_567283); AtNDB3 (NP_193880.5); AtNDB4 (NP_179673); OsNDB (NP_001055220); OsNDB (NP_001058394); PtNDB (XP_002305652); PtNDB (XP_002316663); PtNDB (XP_002319383); PtNDB (XP_002319384); PtNDB (XP_002319927); RcNDB (XP_002517990); RcNDB (XP_002517991); RcNDB (XP_002524685); SbNDB (XP_002438881); SbNDB (XP_002445027); SbNDB (XP_002456448); StNDB (CAB52797); VvNDB (XP_002274469); VvNDB (XP_002274523); VvNDB (XP_002274690); ZmNDB (NP_001142169); SrNDB1; SrNDB2; AmNDB1; AtNDC1 (NP_568205); and OsNDC1 (BAD35311). On the basis of the deduced alignments, the phylogeny of the proteins was inferred using the minimum evolution method, and a rooted phylogenetic tree was obtained by setting the NDC cluster as an out-group. The reliability of the tree was examined using the bootstrap test with 1000 replicates, and branches with partitions reproduced in less than 50 % replicates were collapsed.

Expression analysis of *NDA* and *NDB* transcripts

cDNAs were first generated using a ReverTra Ace qPCR RT (reverse transcription) Kit (Toyobo), and quantitative real-time PCR was then performed with SYBR Green Real-time PCR Master Mix-Plus (Toyobo) using a Thermal Cycler Dice TP800 (Takara Bio). Gene-specific primers were designed against the consensus sequences for both a targeted transcript in *A. maculatum* and its homologue(s) in *S. renifolius*, and used as follows: rtNDAF1-rtNDAR1 for the *NDA* transcripts; rtNDBF1-rtNDBR1 for the *NDB* transcripts; and rtEF1aF1-rtEF1aR1 for the *EF1α* transcripts. PCR was performed using the following conditions: an initial denaturing step at 95 °C for 10 s; 60 amplification cycles of 95 °C for 15 s, 57 °C for 15 s and 72 °C for 30 s; and a dissociation curve analysis at 95 °C for 15 s, 60 °C for 30 s and 95 °C for 15 s. Significant differences between the means were examined by one-way factorial ANOVA and the Tukey's honestly significant difference post-hoc test using SPSS software (IBM).

RESULTS

Respiratory complexes in *S. renifolius* and *A. maculatum*

To characterize the expression profiles of the mitochondrial respiratory complexes in the thermogenic plants *S. renifolius* and *A. maculatum*, mitochondria from stigma-stage spadices of *S. renifolius* and those from δ-stage appendices of *A. maculatum* were isolated. The mitochondrial proteins were then resolved using 1D BN-PAGE after solubilization with various concentrations of digitonin (Figure 1). As shown in the Figure, 1 g of digitonin per g of protein was not sufficient to solubilize
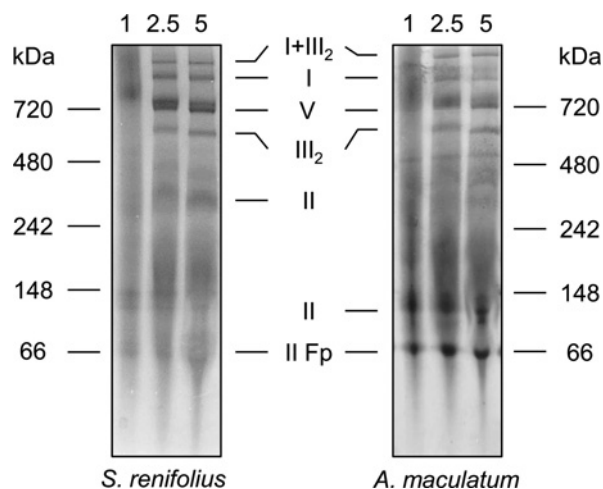
Figure 1   Resolution of mitochondrial protein complexes from *S. renifolius* (left-hand panel) and *A. maculatum* (right-hand panel) after separation by 1D BN-PAGE

Mitochondrial proteins were solubilized using various concentrations of digitonin and were resolved by gel electrophoresis against NativeMark Unstained Protein Standards. Following the electrophoresis, the proteins were visualized by Coomassie Brilliant Blue staining. The digitonin to protein ratios (g/g) are indicated above each lane. Molecular masses of the standard proteins are indicated on the outer sides of the gels. The identities of some visible protein complexes are indicated between the gels and the OXPHOS (oxidative phosphorylation system) complexes are denoted by Roman numerals. The complex II Fp subunit is also individually distinguishable on the gel. The contrast of the original images was manually adjusted to improve the clarity of the protein bands.

either mitochondrial preparation. However, the use of 2.5 or 5 g of digitonin per g of protein worked well in both cases and did not result in different resolutions of the complexes by Coomassie Brilliant Blue staining, with the exceptions of complex V and complex III_2. These two complexes were visualized at slightly lower positions when using 5 g of digitonin. Since Eubel et al. [16] had demonstrated previously that 5 g of digitonin per g of protein is optimal for visualizing complexes in *Arabidopsis* mitochondria, a number of subsequent BN-PAGE studies in plants have employed this concentration. We adopted this dosage in the experiments described below to facilitate a more direct comparison between the results of the present study and previously reported data.

In addition to complex V and complex III_2, bands corresponding to supercomplex $I + III_2$, complex I, complex II and complex II Fp (flavoprotein) subunits were also recognizable on the gel (Figure 1). The identities of the respective bands were first predicted by a comparative approach on the basis of previously published results [16,17] and were later confirmed by gel-based proteomic analysis, as described below. On the whole, the expression and mobility of most of the respiratory complexes on the 1D BN-PAGE gels were very similar between the mitochondria from the two thermogenic plants. The only exception to this was complex II, which in *S. renifolius* mitochondria had drastically less mobility, suggesting a difference in its molecular size. Although it has been widely reported that the mobility of a protein does not correlate well with its molecular mass on a native gel [17], it should be noted that complex II of *S. renifolius* and that of *A. maculatum* had mobilities of 340 kDa and 120 kDa respectively.

2D resolution of respiratory complexes

To further investigate the structures of the respiratory complexes in more detail, their constitutive subunits were separated by 2D

BN/SDS/PAGE (Figure 2) and the protein spots visualized by Coomassie Brilliant Blue staining were further analysed by MS to determine their molecular identities (Table 1). It appears that four known subunits of complex I, namely the 75 kDa, 49 kDa, 39 kDa and 27 kDa proteins, were identified in a lane that corresponds to the position of complex I in the first gel dimension (Figures 2A and 2B). Likewise, four subunits were identified in a lane for complex V; five subunits in a lane for complex III_2; and seven subunits derived from complex I and complex III in a lane for supercomplex $I + III_2$. Heat shock protein 60-like proteins were also detected in lanes for complex V in the mitochondria from both thermogenic plants, as reported previously in yeast mitochondria [25]. Complex II could be characterized by Fp subunits and, when available, iron-sulfur subunit (Ip subunit) on the gels. No notable differences were found in the composition of the respiratory complex subunits between *S. renifolius* and *A. maculatum* mitochondria.

Gel-based proteomic analysis of mitochondrial proteins

Coomassie Brilliant Blue staining visualized approximately 70 2D gel protein spots, regardless of the origin of the mitochondria (Figure 2), and most of these visible spots were subjected to protein identification by MS. We thereby succeeded in identifying approximately 50 proteins for each mitochondrial sample (Figure 2 and Table 1). A total of 44 of these proteins were comparable between the *S. renifolius* and *A. maculatum* mitochondria in terms of their positions on the gels. All of these consensus proteins turned out to be mitochondrial with only one exception, cytosolic aconitase. This is strong evidence that the mitochondria we had prepared were highly purified. A total of 5 proteins were identified as specific for *S. renifolius* mitochondria (A–E in Figure 2 and Table 1). With respect to mitochondrial respiratory components, these included succinate dehydrogenase subunits, which reflect the small mobility of *S. renifolius* complex II in the first gel dimension, and an uncoupling protein [26].

A total of seven proteins were identified as specific for *A. maculatum* mitochondria (a–g in Figure 2 and Table 1). For reasons similar to the case of *S. renifolius* complex II, succinate dehydrogenase Fp subunit was included in this list. Type II NAD(P)H dehydrogenase, which is found on the external face of the mitochondrial inner membrane (NDB) and AOX were also identified as *A. maculatum* mitochondria-specific proteins. The spot corresponding to NDB was clearly recognizable by 2D gel analysis of *A. maculatum* mitochondria (Figure 2B), but appeared to be absent on the *S. renifolius* mitochondria gel (Figure 2A). In the case of AOX, this was also identified as a consensus protein from spot number 13, and the *A. maculatum*-specific identification of this protein was due to its additional distribution on the 2D gel.

Characterization of type II NAD(P)H dehydrogenases in the thermogenic plants

Since the expression status of NDB was found to be different between *S. renifolius* mitochondria and *A. maculatum* mitochondria (Figure 2), we isolated cDNAs encoding type II NAD(P)H dehydrogenases from the thermogenic organs of these two species and analysed the expression levels of these transcripts within the cDNA pools. Using RT–PCR, a cDNA encoding a type II NAD(P)H dehydrogenase found on the internal face of mitochondrial inner membrane (NDA) and a further cDNA encoding NDB were isolated from each plant. The translation initiation codons of the respective transcripts were predicted on the basis of the consensus sequence reported previously [27], and the deduced amino acid sequence of

Table 1   Identified proteins in *S. renifolius* mitochondria and *A. maculatum* mitochondria

+, protein identity was determined by a single experiment; ++, protein identity was determined by two independent experiments; AM, *A. maculatum*; HSP, heat-shock protein; SR, *S. renifolius*.

(a) Protein identities comparable between *S. renifolius* mitochondria and *A. maculatum* mitochondria

Spot ID*	Protein identity	NCBI GI number†		MASCOT score‡		Number of peptide matches§		Determination	
		SR	AM	SR	AM	SR	AM	SR	AM
1	Succinate dehydrogenase flavoprotein subunit	255579273	255087886	304	231	10	8	+	++
2	Aconitase, cytosolic	224133986	255579588	327	519	22	48	++	++
3	α-Keto acid dehydrogenase complex E3 subunit	23321340	211906492	709	493	21	19	++	++
4	Hexokinase	225445080	224143653	119	178	3	5	+	++
5	Type II NAD(P)H dehydrogenase (NDA)	224076814	224116196	101	163	4	7	+	++
6	Serine hydroxymethyltransferase	118489111	222142537	353	158	15	6	++	+
7	Fumarase (class II)	225450679	225437455	113	515	8	14	+	++
8	Citrate synthase	325301868	40646744	566	148	18	9	++	++
9	NAD-dependent malate dehydrogenase	21388550	21388550	2082	1183	15	13	++	++
10	Manganese superoxide dismutase	226693990	226693990	101	54	2	1	+	+
11	Dicarboxylate/tricarboxylate translocator	19913109	1100739	261	189	5	11	+	++
12	Adenine nucleotide translocator	225435480	1890116	504	428	36	31	++	++
13	Alternative oxidase	57157824	308153038	158	713	12	53	+	++
14	Dicarboxylate carrier protein	13878155	225459119	165	455	7	15	+	++
15	Pyruvate dehydrogenase complex E1 α-subunit	12003246	211906500	399	305	16	22	++	++
16	Pyruvate dehydrogenase complex E1 β-subunit	326490341	115480067	1085	319	12	9	++	++
17	Glutamate dehydrogenase	115455879	224145986	259	119	19	13	++	+
18	2-Oxoglutarate dehydrogenase complex E1 subunit	297794187	225449605	441	625	25	41	+	++
19	NAD-dependent malic enzyme α- and/or β-subunit	224136522	224067419	630	487	35	16	++	++
20	COX subunit 2	23095854	23095854	180	228	9	5	+	++
21	Mitochondrial processing peptidase β-subunit	147765656	147765656	169	208	14	20	++	++
22	Mitochondrial processing peptidase α-subunit	225442426	225442426	562	265	9	4	++	++
23	Cytochrome b−c1 complex cytochrome c1 (subunit 4)	195614944	224131844	200	217	7	13	++	++
24	Cytochrome b−c1 complex 14kDa protein (subunit 7)	15239430	15239430	103	68	6	4	+	+
25	Cytochrome b−c1 complex QP-C (subunit 8)	115466706	115466706	112	109	2	2	+	++
26	Chaperonin HSP60	255554262	255554262	1143	1097	67	75	++	++
27	ATP synthase α-subunit (F$_1$)	34539393	6561666	2201	873	66	39	++	++
28	ATP synthase β-subunit (F$_1$)	115465323	222632492	4333	2225	53	54	++	++
29	ATP synthase γ-subunit (F$_1$)	255581367	195644888	221	106	9	1	++	++
30	ATP synthase D-chain (F$_o$)	15231176	255570779	103	100	8	11	+	++
31	NADH-ubiquinone oxidoreductase 75 kDa protein	255582280	195648210	298	451	14	13	++	++
32	NADH-ubiquinone oxidoreductase 49 kDa protein	44889037	44889037	283	382	9	8	+	++
33	NADH-ubiquinone oxidoreductase 39 kDa protein	225437963	255571168	172	192	8	9	+	++
34	NADH-ubiquinone oxidoreductase 27 kDa protein	9280612	9280612	315	229	16	8	+	+
35	Prohibitin	225462272	255637310	723	1158	19	12	++	++
36	NADH-ubiquinone oxidoreductase 75 kDa protein	255582280	224069170	556	397	10	16	++	++
37	Mitochondrial processing peptidase β-subunit	12802327	12802327	205	105	10	16	++	++
38	Mitochondrial processing peptidase α-subunit	225442426	225442426	593	183	7	3	++	+
39	NADH-ubiquinone oxidoreductase 49 kDa protein	44889037	44889037	628	266	10	7	++	+
40	NADH-ubiquinone oxidoreductase 39kDa protein	224132264	255571168	228	160	12	6	++	+
41	Cytochrome b−c1 complex cytochrome c1 (subunit 4)	195614944	224131844	204	275	6	11	+	+
42	NADH-ubiquinone oxidoreductase 75 kDa protein	9280612	742345	423	128	18	8	+	+
43	2-Oxoglutarate dehydrogenase complex E1 subunit	225449605	255575120	431	570	27	30	+	++
44	2-Oxoglutarate dehydrogenase complex E2 subuinit	294463753	224116582	56	398	2	12	+	++

(b) Protein identities specific to *S. renifolius* mitochondria

Spot ID*	Protein identity	NCBI GI number†		MASCOT score‡		Number of peptide matches§		Determination	
		SR	AM	SR	AM	SR	AM	SR	AM
A	Succinate dehydrogenase flavoprotein subunit	255579273	—	1291	—	23	—	++	—
B	Succinate dehydrogenase iron–sulfur subunit	224055647	—	113	—	4	—	++	—
C	Voltage-dependent anion exchange carrier	115438000	—	251	—	3	—	+	—
D	Pyruvate dehydrogenase complex E2 subuinit	115471693	—	155	—	10	—	+	—
E	Uncoupling protein	7106159	—	184	—	7	—	++	—

(c) Protein identities specific to *A. maculatum* mitochondria

Spot ID*	Protein identity	NCBI GI number†		MASCOT score‡		Number of peptide matches§		Determination	
		SR	AM	SR	AM	SR	AM	SR	AM
a	Succinate dehydrogenase flavoprotein subunit	—	224134312	—	1032	—	34	—	++
b	Type II NAD(P)H dehydrogenase (NDB)	—	5732076	—	154	—	11	—	++

Table 1   Continued

Spot ID*	Protein identity	NCBI GI number†		MASCOT score‡		Number of peptide matches§		Determination	
		SR	AM	SR	AM	SR	AM	SR	AM
c	NAD-dependent isocitrate dehydrogenase α-subunit	–	115435934	–	493	–	10	–	++
d	Alternative oxidase	–	308153046	–	390	–	32	–	++
e	Voltage-dependent anion exchange carrier	–	242058515	–	104	–	8	–	++
f	T25K16.16 (stress-inducible)	–	6715639	–	342	–	1	–	++
g	Hexokinase	–	224143653	–	1103	–	7	–	++

*Numbers or letters given to each protein identity in this Table correspond to those marked in Figure 2.

†A NCBI GI number refers to an amino acid sequence that had the highest protein score in each MASCOT MS/MS ion search. When two independent experiments assigned different GI numbers to queries derived from the same protein, the one with higher protein score was employed. In some cases where a set of peptide sequences in a query corresponds to multiple amino acid sequences, only one GI number is shown in this Table.

‡The highest protein scores in respective MASCOT MS/MS ion searches are listed. When two independent experiments gave different scores to a single protein, the higher one was employed.

§The number of non-duplicate peptide matches within the same protein family is given to each protein identification. When two independent experiments gave different results, the one with higher protein score was employed.

each transcript was generated (Supplementary Figures S1 and S2 at http://www.BiochemJ.org/bj/445/bj4450237add.htm). AmNDA1 and two SrNDAs were theoretically determined to be 61 kDa proteins in their precursor forms. However, they were predicted to form 54 kDa mature proteins after the putative mitochondrial targeting sequences predicted by Mitoprot were cleaved (Supplementary Figure S1). These predicted molecular masses are in good agreement with the 2D mobilities found by 2D BN/SDS/PAGE in which the NDA protein bands always appeared at approximately 54 kDa (Figure 2). AmNDB1 and two SrNDBs were predicted to be 65 kDa proteins in their precursor forms. Mitoprot further predicted that, although AmNDB1 would be processed into a 61 kDa protein, SrNDB1 and SrNDB2 would be processed into 63 kDa proteins (Supplementary Figure S2). Molecular mass estimates for the NDB protein spot from *A. maculatum* mitochondria was consistently determined to be 62 kDa (Figure 2B).

When aligned with previously characterized type II NAD(P)H dehydrogenases from potato, several functional motifs were identified in the dehydrogenases from *S. renifolius* and *A. maculatum*. Two dinucleotide-fold fingerprints, which have been reported to be well conserved in both NDAs and NDBs, were found in the amino acid sequences of the newly identified sequences (Figure 3A) [28,29]. In addition, the Ca^{2+}-binding EF-hand motif first identified in potato NDB [28] was found to be conserved among the NDB sequences in the present study (Figure 3B). Another EF-hand motif reported previously in *Neurospora crassa* p64, a homologue of plant NDB, was not found in any of the NDB sequences [30]. Phylogenetic analysis of 15 plant NDA sequences, 22 plant NDB sequences and two plant NDC sequences clearly demonstrated the identities of the dehydrogenases from *S. renifolius* and *A. maculatum* as they were grouped into their respective protein families (Figure 3C). Intriguingly, the distribution of monocot- and dicot-derived dehydrogenases within this phylogenetic tree suggested the possibility that at least two subfamilies exist in each protein family.

Expression abundance of *NDA* and *NDB* transcripts in various thermogenic organs

The expression levels of transcripts encoding NDA and NDB were investigated in a spadix of *S. renifolius* and an appendix of *A. maculatum*, as well as in leaves and spathes of both species (NDA in Figure 3D and NDB in Figure 3E). Since this analysis

could not discriminate between two homologous SrNDAs nor the two SrNDBs, the quantities of *NDA* and *NDB* in the samples from *S. renifolius* represent the gross expression levels of the two homologues in the respective gene families. Figure 3(D) reveals that *NDA* was expressed to the same degree in the two thermogenic organs. In non-thermogenic organs, however, *NDA* expression levels tended to be lower. On the other hand, *NDB* showed a significantly higher expression in the appendix of *A. maculatum* than in the spadix of *S. renifolius*. Furthermore, expression levels of *NDB* in the spadix and the spathe were comparable in *S. renifolius*. In the other non-thermogenic organs, the expression levels of *NDB* tended to be much lower.

Native structure of AOX in *S. renifolius* and *A. maculatum*

Since AOX has been proposed to function in both homoeothermic thermogenesis in *S. renifolius* [21] and in transient thermogenesis in *A. maculatum* [7,12], its native structure in each plant was investigated. On a 1D image, AOX was detectable as a broad smear with a densitometric peak at approximately 200 kDa in both species (Figure 4A), the appearance of which was not largely affected by digitonin concentration or freeze–thaw treatments at least in *S. renifolius* (Supplementary Figure S3 at http://www.BiochemJ.org/bj/445/bj4450237add.htm). Mitochondria from non-transformed *S. pombe* and those from its transformant expressing AmAOX1e, the most abundantly expressed AOX in the appendices of *A. maculatum* [7], were also analysed as negative and positive controls, respectively (Supplementary Figure S4 at http://www.BiochemJ.org/bj/445/bj4450237add.htm). No signal was detected in the former, but a signal at approximately 200 kDa appeared very clearly in the latter.

AOX was detected as a horizontally broad smear at approximately 35 kDa in the 2D analysis, and in addition a minor smear at approximately 70 kDa was also recognizable (*S. renifolius* in Figure 4B and *A. maculatum* in Figure 4C). We suggest that this minor smear is derived from an oxidized form of AOX that had not been reduced sufficiently by reductive alkylation of a 1D gel strip. Obscure distribution of AOX in 2D BN/SDS/PAGE has previously been reported in non-thermogenic plants, namely *Arabidopsis* and *Phaseolus vulgaris* [16], as well as in thermogenic *A. maculatum* [19]. In the former report, the smear-like signals appeared at between 30 kDa and 300 kDa in the first dimension, whereas the latter study described signals of below 50 kDa. In contrast with the results of the latter report
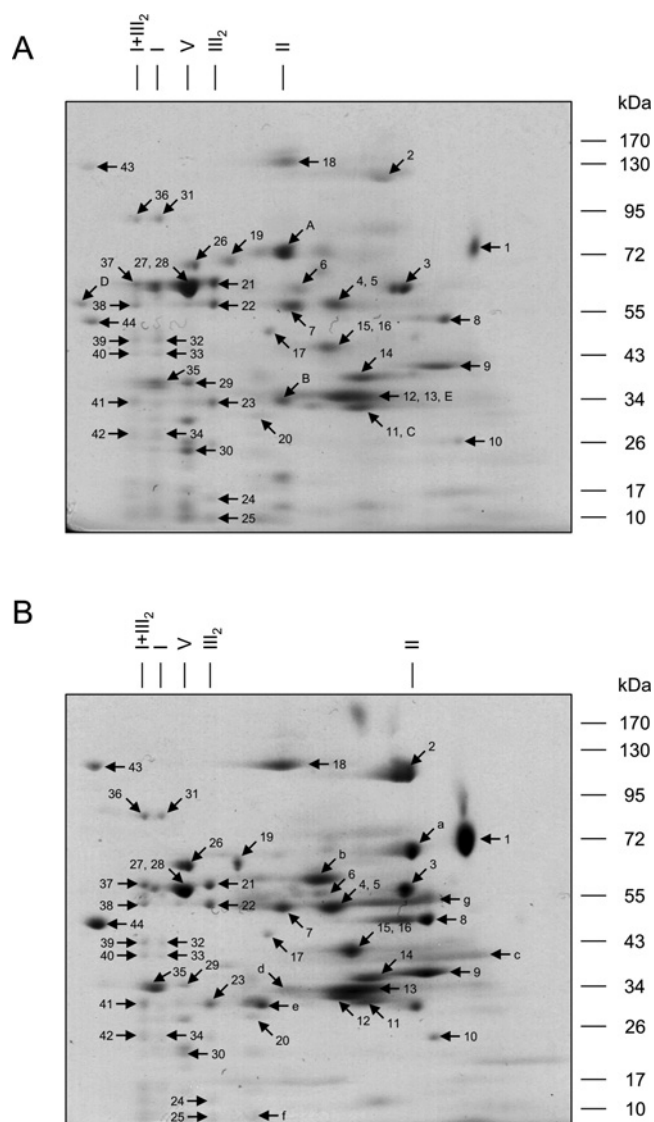
Figure 2   2D resolution of the mitochondrial complexes in *S. renifolius* (A) and *A. maculatum* (B) after separation by 2D BN/SDS/PAGE

Mitochondrial proteins were solubilized by digitonin (5 g/g of protein) prior to 1D BN-PAGE, and then reduced and alkylated prior to 2D SDS-PAGE. The proteins were stained using Coomassie Brilliant Blue. Molecular masses of standard proteins in the second dimension are indicated to the right-hand side of the gels. The identities of the protein complexes specified in Figure 1 are indicated above the gels. Arrows mark the proteins identified by MS. Numbers and letters attached to the arrows correspond to those used for the respective protein identities listed in Table 1. The contrast and brightness of the original images were manually adjusted for maximum clarity.

[19], our present analysis detected a smear-like signal of *A. maculatum* AOX in a much higher molecular mass region in the first dimension, which was quite similar to the observation made in the non-thermogenic plants [16]. This result was also supported by mass-spectrometric identification of the AOX protein on 2D BN/SDS/PAGE gels (Figure 2 and Table 1).

DISCUSSION

Some plants are known to undergo floral development accompanied by organ-specific thermogenesis. In Araceae, the stigma-stage spadices of *S. renifolius* were previously reported

to show homoeothermic activity [8], whereas the δ-stage appendices of *A. maculatum* are known to raise their temperatures transiently [5]. Although increased respiratory activities via the energy-dissipative AOX have been shown to correlate with thermogenesis in both species [12,21], the molecular bases for their different thermogenic properties have not been well characterized. Hence, in the present study, we comparatively analysed the expressions and native structures of respiratory components within mitochondria isolated from the thermogenic organs of *S. renifolius* and *A. maculatum*.

In addition to four of the five typical respiratory complexes, namely complex I, II, III_2 and V, supercomplex $I+III_2$ was identified in the mitochondria from each plant (Figure 1 and Figure 2). This supercomplex has been reported to be expressed abundantly in various non-thermogenic plants, where 50%–90% of complex I is integrated into this supercomplex [16]. In the case of thermogenic plants, a previous study has reported that all detectable complex I forms a supercomplex in *A. maculatum* [19], whereas only 60% was found to do so from our present results. This inconsistency may derive from different storage conditions or different numbers of freeze–thaw cycles that the mitochondria had to experience, as the amount of some supercomplexes has been reported to be significantly affected by these factors [16]. In any case, the high abundance of supercomplex $I+III_2$, which probably contributes to the substrate channeling of the COX (cytochrome *c* oxidase)-mediated respiratory pathway, suggests that AOX mainly utilizes reducing equivalents from ubiquinone reductases other than complex I in *S. renifolius* and *A. maculatum*.

Besides complexes I and II, two NAD(P)H dehydrogenases are known to constitute the mitochondrial respiratory chain in plants which reduce ubiquinone to ubiquinol without any net proton translocation across the inner membrane [31]. In the present study, NDB, the NAD(P)H dehydrogenase expressed on the external surface of the inner membrane, was found to be abundant in the appendices of *A. maculatum*, but not in the spadices of *S. renifolius* (Figure 2). This was also confirmed at the transcript level (Figure 3E). Such results suggest that NDB supplies a great deal of reducing power from a cytosolic NAD(P)H pool to the mitochondrial respiratory chain or, more speculatively, to AOX in the appendices of *A. maculatum*. In this regard, high rates of glycolysis have been reported in the thermogenic spadices of *A. maculatum* in association with increased maximum catalytic activities of the glycolytic enzymes [32]. Moreover, it was previously reported that the oxygen consumption rate of AOX is 2.3-fold higher than that of COX in mitochondria isolated from spadices of *A. maculatum* when NADH was externally added as a respiratory substrate at 21 °C [33]. Hence, the availability of exogenous NADH, which is probably linked to glycolytic activity in the cytosol, is an important factor underlying the high respiratory activity of AOX in this plant.

The other NAD(P)H dehydrogenase, the so-called NDA enzyme, was identified in the mitochondria from both plant species (Figure 2), and expression levels of the corresponding transcript(s) appeared comparable (Figure 3D). This suggests both *S. renifolius* and *A. maculatum* utilize this enzyme to provide reducing equivalents to the ubiquinone pool; however, *S. renifolius*, with less abundance of NDB, may depend more on NDA than *A. maculatum*. In *S. renifolius*, the difference between the floral and ambient temperature has been found to show a positive correlation with CO_2 production in the regulation of floral temperature [34]. As the CO_2 is presumably produced during TCA (tricarboxylic acid) cycle activity, the re-oxidation of NADH within the mitochondrial compartment is vital for maintaining cycle turnover, particularly at low ambient temperatures. Hence it
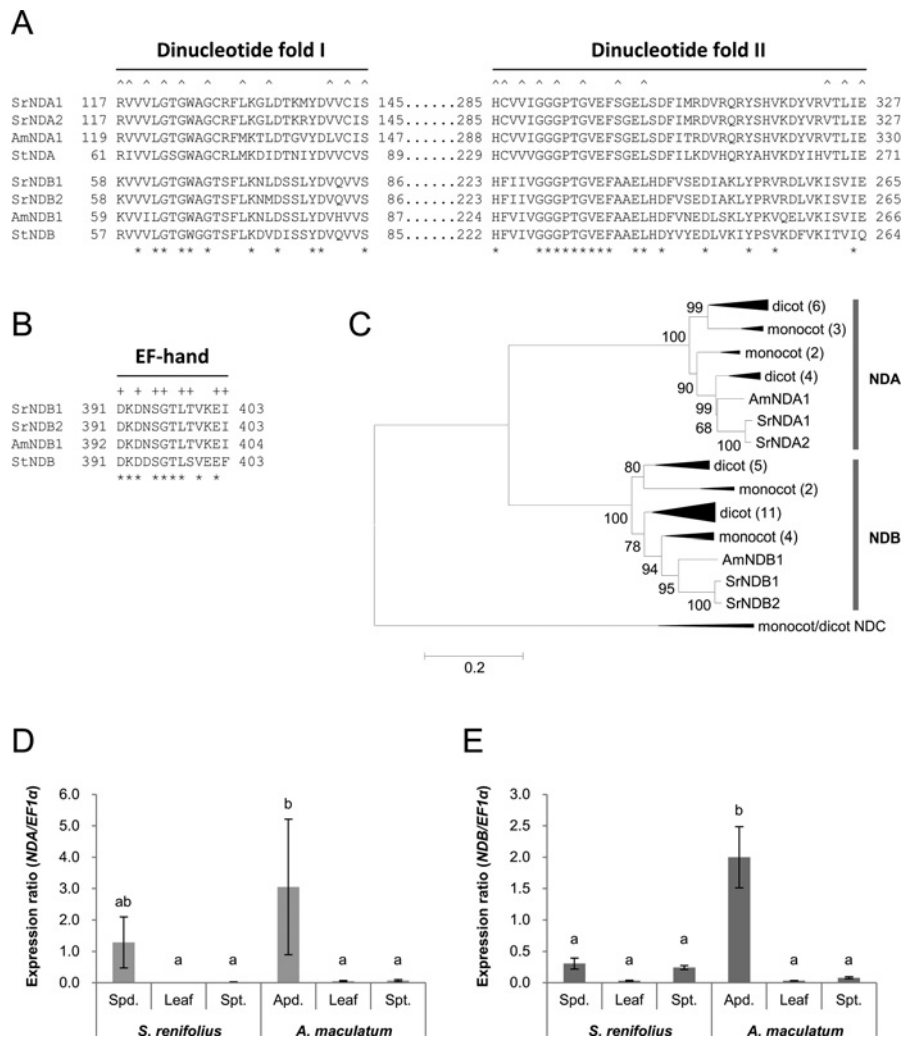
Figure 3   Characterization of the deduced amino acid sequences of the type II NAD(P)H dehydrogenases derived from *S. renifolius* and *A. maculatum*, and the organ-specific expression profiles of these transcripts in each respective species

(**A**) A total of two dinucleotide-fold fingerprints, the hallmarks of the type II NAD(P)H dehydrogenases, in the newly identified sequences are shown in alignment with StNDA and StNDB. Asterisks indicate conserved amino acid residues. Circumflex accents (^) above the alignment indicate positions corresponding to the fingerprints. (**B**) A Ca^{2+}-binding EF-hand motif identified in SrNDBs and AmNDB is shown in the same manner as in (**A**). Plus signs ($+$) above the alignment indicate positions of the motif. (**C**) The phylogeny of the proteins was inferred using the minimum evolution method, and its reliability was examined via the bootstrap test with 1000 replicates. Partitions reproduced in less than 50 % of the replicates of the test were collapsed. The percentage of replicated trees in which associated taxa clustered together in the test is shown for each significant node. The tree is drawn to scale, reflecting the evolutionary distances used to infer the phylogeny. Each number in parentheses represents the number of sequences in a compressed subtree. A small number of NDC sequences were included as an out-group. (**D**) Expression levels of *NDA* transcripts in three different organs of both *S. renifolius* and *A. maculatum* were analysed. *EF1α* transcripts were used as a normalization control. The *NDA/EF1α* ratios can be compared not only across different organs within a species, but also across species. A total of three biological replications were analysed. Different letters marked above the bars indicate statistical significance between one another (Tukey's honestly significant differences post-hoc test; $n = 3$; $P < 0.05$). Apd, appendix; Spd, spadix; Spt, spathe. (**E**) Expression level of *NDB* transcripts analysed in the same manner as the *NDA* transcripts in panel (**D**).

is interesting to speculate that, in homoeothermic plants, perhaps NDA plays a more important role in the maintenance of TCA cycle activity.

Complex II is another crucial factor in the respiratory chain and in the TCA cycle. Interestingly, the molecular mass of this complex seems to be drastically different between the mitochondria from *S. renifolius* and those from *A. maculatum* (Figure 1). In *A. maculatum*, complex II had an apparent molecular mass of 120 kDa. This is similar to porcine complex II (124 kDa) [35] and *Escherichia coli* succinate:ubiquinone oxidoreductase (120 kDa), a prokaryotic homologue of mitochondrial complex II [36]. Both of them consist of four common subunits, but are slightly smaller than complex II of other plants [16]. Complex II has been reported to be 150 kDa

in *Arabidopsis*, potato and *P. vulgaris* because they contain four additional plant-specific subunits, namely SDH5, SDH6, SDH7 and SDH8 [18]. Although homologues of these subunits seem to be conserved in monocots as well (results not shown), complex II of *A. maculatum* has been reported as a four-subunit complex instead of the eight-subunit complex described in a previous study [19]. Hence the cumulative evidence could be interpreted in two ways: (i) complex II of *A. maculatum* is indeed 120 kDa *in vivo* and the four plant-specific subunits are not necessary for its functionality; or (ii) complex II is actually 150 kDa *in vivo*, but appears as a 120 kDa complex on the gel owing to either partial dissection of the original form or a fast migration in native PAGE. In either case, complex II of *A. maculatum* probably exists in a monomeric form, as found in most organisms investigated to date.
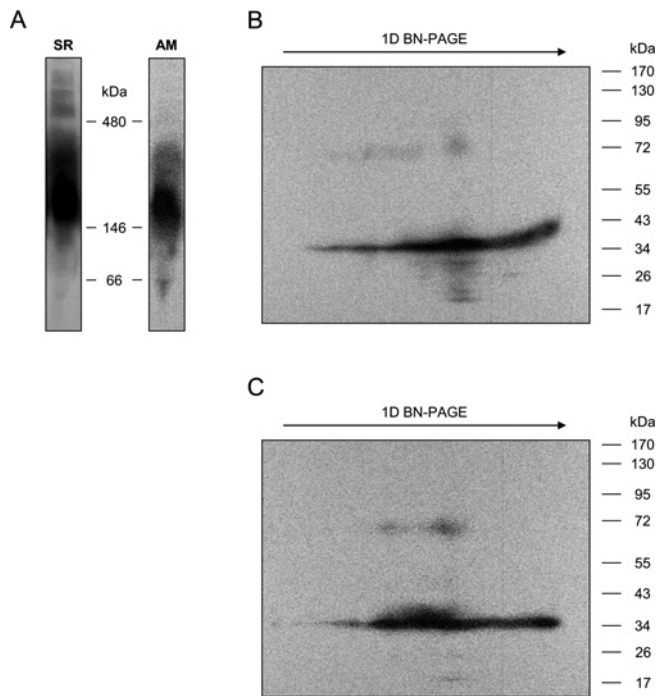
Figure 4 Immunological identification of AOX in the mitochondria of both _S. renifolius_ and _A. maculatum_ following either 1D BN-PAGE or 2D BN/SDS/PAGE

(**A**) AOX was detected on a membrane on to which the mitochondrial proteins separated by 1D BN-PAGE had been blotted. AM, _A. maculatum_ mitochondria; SR, _S. renifolius_ mitochondria. Molecular masses of the standard proteins in the first dimension are indicated between the two images. _S. renifolius_ AOX (SrAOX) was detected in two independent experiments and similar results were obtained. For _A. maculatum_ AOX (AmAOX), a single experiment was conducted. (**B**) SrAOX was detected on a membrane on to which the proteins separated by 2D BN/SDS/PAGE had been blotted. Molecular masses of standard proteins in the second dimension are indicated to the right-hand side of the image. An arrow drawn above the image indicates the direction of the 1D BN-PAGE. A single experiment was conducted. (**C**) AmAOX was detected in exactly the same manner as in (**B**).

Complex II of _S. renifolius_ has an apparent molecular mass of 340 kDa. This is a very unusual size for this protein, in both plants and other organisms, because such a large molecular mass usually infers an oligomeric or a supramolecular structure. Thus far, however, complex II has never been shown to be an oligomer _in vivo_ and has rather been reported as a monomer in yeast, mammals and plants [16,37]. The only report thus far that has shown evidence for an oligomeric structure of complex II was a report on the _E. coli_ homologue, which suggested the complex may form a trimer under physiological conditions on the basis of its crystallographic packaging [36]. The supramolecular structure of complex II has not yet been elucidated either. However, several large versions of complex II have been detected weakly, but distinctly, by _in gel_ activity staining of _A. maculatum_ mitochondria [19]. Hence, a possibility that complex II exists as a trimer or a supercomplex in the spadices of _S. renifolius_ cannot be ruled out at present and will require clarification in future studies.

No multiprotein complex comprising AOX has been identified to date, although the native structure of this energy-dissipative oxidase has already been analysed by BN-PAGE in _Arabidopsis_, _P. vulgaris_ and _A. maculatum_ [16,19]. However, the authors of these studies have inferred that AOX does not form a supercomplex and that smear-like signals of AOX in the first dimension are derived from aggregates of this enzyme. In _A. maculatum_, the smear was previously reported to appear below

50 kDa in the first dimension, but in the present study was detected in the 150–350 kDa ranges (Figure 4). AmAOX1e expressed in yeast also appears at approximately 200 kDa in the native condition (Supplementary Figure S4), suggesting that even in this heterologous system the same AOX-comprising complex is also apparent. In addition, the pattern of the smear was not significantly affected by the concentration of digitonin or freeze–thaw cycles in the case of _S. renifolius_ AOX (Supplementary Figure S3). Therefore we speculate that the smear at approximately 200 kDa is not derived from an aggregation of the protein, but rather reflects a specific physiological situation.

In general, the expression profiles of the respiratory complexes, supercomplexes and other mitochondrial proteins that we investigated in our present study were very similar between _S. renifolius_ and _A. maculatum_. However, several important members of the respiratory chain, such as NDB and complex II, were shown to have a different expression status between these plant species, and they may therefore play a crucial role in their respective thermogenic pathways, particularly in the regulation of electron flow to the respiratory chain. If this is indeed the case, such a key enzyme would be expected to regulate the metabolic flux with greater precision in the case of _S. renifolius_ and to boost the flux up to its maximum capacity in the case of _A. maculatum_. In fact, the reduction level of the ubiquinone pool in the stigma-stage spadices of _S. renifolius_ remains in the range of 40–75% [10], whereas that in the δ-stage appendices of _A. maculatum_ reaches approximately 90% [5]. Hence it is important to study not only the native structures of these respiratory enzymes, but also the functional differences between species in order to properly elucidate the metabolic regulator in _S. renifolius_ or the metabolic booster in _A. maculatum_.

REFERENCES

1 Skubatz, H., Nelson, T. A., Dong, A. M., Meeuse, B. J. D. and Bendich, A. J. (1990) Infrared thermography of _Arum_ lily inflorescences. Planta **182**, 432–436

2 Seymour, R. S. and Schultze-Motel, P. (1996) Thermoregulating lotus flowers. Nature **383**, 305

3 Skubatz, H., Tang, W. and Meeuse, B. J. D. (1993) Oscillatory heat-production in the male cones of cycads. J. Exp. Bot. **44**, 489–492

4 Meeuse, B. J. D. (1975) Thermogenic respiration in aroids. Ann. Rev. Plant Physiol. **26**, 117–126

5 Wagner, A. M., Wagner, M. J. and Moore, A. L. (1998) _In vivo_ ubiquinone reduction levels during thermogenesis in Araceae. Plant Physiol. **117**, 1501–1506

6 Bermadinger-Stabentheiner, E. and Stabentheiner, A. (1995) Dynamics of thermogenesis and structure of epidermal tissues in inflorescences of _Arum maculatum_. New Phytol. **131**, 41–50

7   Ito, K., Ogata, T., Kakizaki, Y., Elliott, C., Albury, M. S. and Moore, A. L. (2011) Identification of a gene for pyruvate-insensitive mitochondrial alternative oxidase expressed in the thermogenic appendices in *Arum maculatum*. Plant Physiol. **157**, 1721–1732

8   Uemura, S., Ohkawara, K., Kudo, G., Wada, N. and Higashi, S. (1993) Heat-production and cross-pollination of the Asian skunk cabbage *Symplocarpus renifolius* (Araceae). Am. J. Bot. **80**, 635–640

9   Ito, K., Onda, Y., Sato, T., Abe, Y. and Uemura, M. (2003) Structural requirements for the perception of ambient temperature signals in homeothermic heat production of skunk cabbage (*Sympocarpus foetidus*). Plant Cell Environ. **26**, 783–788

10 Kamata, T., Matsukawa, K., Kakizaki, Y. and Ito, K. (2009) *In vivo* redox state of the ubiquinone pool in the spadices of the thermogenic skunk cabbage, *Symplocarpus renifolius*. J. Plant Res. **122**, 645–649

11 Affourtit, C., Albury, M. S., Crichton, P. G. and Moore, A. L. (2002) Exploring the molecular nature of alternative oxidase regulation and catalysis. FEBS Lett. **510**, 121–126

12 Leach, G. R., Krab, K., Whitehouse, D. G. and Moore, A. L. (1996) Kinetic analysis of the mitochondrial quinol-oxidizing enzymes during development of thermogenesis in *Arum maculatum* L. Biochem. J. **317**, 313–319

13 Grant, N. M., Miller, R. E., Watling, J. R. and Robinson, S. A. (2008) Synchronicity of thermogenic activity, alternative pathway respiratory flux, AOX protein content, and carbohydrates in receptacle tissues of sacred lotus during floral development. J. Exp. Bot. **59**, 705–714

14 Rhoads, D. M. and McIntosh, L. (1992) Salicylic acid regulation of respiration in higher plants: alternative oxidase expression. Plant Cell **4**, 1131–1139

15 Eubel, H., Braun, H. P. and Millar, A. H. (2005) Blue-native PAGE in plants: a tool in analysis of protein-protein interactions. Plant Methods **1**, 11–23

16 Eubel, H., Jänsch, L. and Braun, H. P. (2003) New insights into the respiratory chain of plant mitochondria. Supercomplexes and a unique composition of complex II. Plant Physiol. **133**, 274–286

17 Eubel, H., Heinemeyer, J. and Braun, H. P. (2004) Identification and characterization of respirasomes in potato mitochondria. Plant Physiol. **134**, 1450–1459

18 Millar, A. H., Eubel, H., Jänsch, L., Kruft, V., Heazlewood, J. L. and Braun, H. P. (2004) Mitochondrial cytochrome *c* oxidase and succinate dehydrogenase complexes contain plant specific subunits. Plant Mol. Biol. **56**, 77–90

19 Sunderhaus, S., Klodmann, J., Lenz, C. and Braun, H. P. (2010) Supramolecular structure of the OXPHOS system in highly thermogenic tissue of *Arum maculatum*. Plant Physiol. Biochem. **48**, 265–272

20 James, W. O. and Beevers, H. (1950) The respiration of *Arum* spadix. A rapid respiration, resistant to cyanide. New Phytol. **49**, 353–374

21 Onda, Y., Kato, Y., Abe, Y., Ito, T., Ito-Inaba, Y., Morohashi, M., Ito, Y., Ichikawa, M., Matsukawa, K., Otsuka, M. et al. (2007) Pyruvate-sensitive AOX exists as a non-covalently associated dimer in the homeothermic spadix of the skunk cabbage, *Symplocarpus renifolius*. FEBS Lett. **581**, 5852–5858

22 Moore, A. L., Fricaud, A. C., Walters, A. J. and Whitehouse, D. G. (1993) Isolation and purification of functionally intact mitochondria from plant cells. Methods Mol. Biol. **19**, 133–139

23 Moore, A. L., Walters, A. J., Thorpe, J., Fricaud, A. C. and Watts, F. Z. (1992) *Schizosaccharomyces pombe* mitochondria: morphological, respiratory and protein import characteristics. Yeast **8**, 923–933

24 Tamura, K., Dudley, J., Nei, M. and Kumar, S. (2007) MEGA4: molecular evolutionary genetics analysis (MEGA) software version 4.0. Mol. Biol. Evol. **24**, 1596–1599

25 Gray, R. E., Grasso, D. G., Maxwell, R. J., Finnegan, P. M., Nagley, P. and Devenish, R. J. (1990) Identification of a 66 KDa protein associated with yeast mitochondrial ATP synthase as heat shock protein hsp60. FEBS Lett. **268**, 265–268

26 Ito, K. (1999) Isolation of two distinct cold-inducible cDNAs encoding plant uncoupling proteins from the spadix of skunk cabbage (*Symplocarpus foetidus*). Plant Sci. **149**, 167–173

27 Joshi, C. P., Zhou, H., Huang, X. and Chiang, V. L. (1997) Context sequences of translation initiation codon in plants. Plant Mol. Biol. **35**, 993–1001

28 Rasmusson, A. G., Svensson, A. S., Knoop, V., Grohmann, L. and Brennicke, A. (1999) Homologues of yeast and bacterial rotenone-insensitive NADH dehydrogenases in higher eukaryotes: two enzymes are present in potato mitochondria. Plant J. **20**, 79–87

29 Kerscher, S. J. (2000) Diversity and origin of alternative NADH:ubiquinone oxidoreductases. Biochim. Biophys. Acta **1459**, 274–283

30 Melo, A. M. P., Duarte, M. and Videira, A. (1999) Primary structure and characterization of a 64 kDa NADH dehydrogenase from the inner membrane of *Neurospora crassa* mitochondria. Biochim. Biophys. Acta **1412**, 282–287

31 Rasmusson, A. G., Soole, K. L. and Elthon, T. E. (2004) Alternative NAD(P)H dehydrogenases of plant mitochondria. Ann. Rev. Plant Biol. **55**, 23–39

32 ap Rees, T., Wright, B. W. and Fuller, W. A. (1977) Measurements of starch breakdown as estimates of glycolysis during thermogenesis by the spadix of *Arum maculatum* L. Planta **134**, 53–56

33 Cook, N. D. and Cammack, R. (1985) Effects of temperature on electron transport in *Arum maculatum* mitochondria. Plant Physiol. **79**, 332–335

34 Seymour, R. S., Lindshau, G. and Ito, K. (2010) Thermal clamping of temperature-regulating flowers reveals the precision and limits of the biochemical regulatory mechanism. Planta **231**, 1291–1300

35 Sun, F., Huo, X., Zhai, Y., Wang, A., Xu, J., Su, D., Bartlam, M. and Rao, Z. (2005) Crystal structure of mitochondrial respiratory membrane protein complex II. Cell **121**, 1043–1057

36 Yankovskaya, V., Horsefield, R., Törnroth, S., Luna-Chavez, C., Miyoshi, H., Léger, C., Byrne, B., Cecchini, G. and Iwate, S. (2003) Architecture of succinate dehydrogenase and reactive oxygen species generation. Science **299**, 700–704

37 Schägger, H. and Pfeiffer, K. (2000) Supercomplexes in the respiratory chains of yeast and mammalian mitochondria. EMBO J. **19**, 1777–1783

SUPPLEMENTARY ONLINE DATA
Different molecular bases underlie the mitochondrial respiratory activity in the homoeothermic spadices of *Symplocarpus renifolius* and the transiently thermogenic appendices of *Arum maculatum*

Yusuke KAKIZAKI*, Anthony L. MOORE† and Kikukatsu ITO‡[1]

*The United Graduate School of Agricultural Sciences, Iwate University, 3-18-8 Ueda, Morioka, Iwate, 020-8550, Japan, †Department of Biochemistry and Molecular Biology, School of Life Sciences, University of Sussex, Falmer, Brighton, BN1 9QG, U.K., and ‡Cryobiofrontier Research Center, Faculty of Agriculture, Iwate University, 3-18-8 Ueda, Morioka, Iwate, 020-8550, Japan

```
SrNDA1    1 MGFSRIARSALRQSPGTNPASRIPSSNYMNQTASHCEGLPQSG--SYFFSVRYITTNSTLKHLP-SVGTMDRLSFESRGI  77
SrNDA2    1 MGFSRIARSALRQSPGTNPASRIPSSNYMNQTASHCKGLPQSG--SYFFSVRYITTNSTLKHLP-SVGTMDRLSFESRGI  77
AmNDA1    1 MGLSKIARSAWKTSLSADSVNRMLGSGHVIQTSVLLGDLLPSSARHHLLLARFVTTTGSTQRHPPGFESRDCEDRGSRGI  80
            **  * *****  *        *   *   **   *  *        * **     *       *     *    ****

SrNDA1   78 SVTPQRQFPLAERVEEDPEVEVESRRLPGLGATKPGEKPRVVVLGTGWAGCRFLKGLDTKMYDVVCISPRNHMVFTPLLA 157
SrNDA2   78 SVTPQRQFPLAERVEEDSEVEVESRSLRGLGATKPGEKPRVVVLGTGWAGCRFLKGLDTKRYDVVCISPRNHMVFTPLLA 157
AmNDA1   81 SVTPHRQSPLAQPVEEEPDVENDRRQA-GLEATRPGEKPRVVVLGTGWAGCRFMKTLDTGVYDLVCISPRNHMVFTPLLA 159
            **** ** ***  ***   **    *   ** ** ************** ** *** **  *  ** ***************
                                             ++ + + +  +   + +          + - -

SrNDA1  158 STCVGTLEFRSVAEPVSQIQAALGGAPNSYFYLASCMGIDTDKHEVYCEAVPG-AGLPNEPYGFTVAYDKLVIAAGAEPL 236
SrNDA2  158 STCVGTLEFRSVAEPVSQIQAALGGAPNSYFYLASCMGIDTDKHEVYCEAVPG-AGLPNEPYRFSVAYDKLVIAAGAEPL 236
AmNDA1  160 STCVGTLEFRSVAEPVSRIQTALATAPNSYFYLASCNGIDVDRHEVYCEAVPSSVGLSTEPYKFKVAYDKLVIAAGADPL 239
            *****************  **  **  ********** *** *  ********    **  *** * ********* **

SrNDA1  237 TFNIKGVKEHAFFLREVNHAQEIRKKLLLNLMLSENPGISEEEKNRLLHCVVIGGGPTGVEFSGELSDFIMRDVRQRYSH 316
SrNDA2  237 TFNIKGVKEHAFFLREVNHAQEIRKKLLLNLMLSENPGISEEEKKRLLHCVVIGGGPTGVEFSGELSDFIMRDVRQRYSH 316
AmNDA1  240 TFNIKGVKEHAFFLREVNHAQEIRKKLLLNLMLSDNPGVSEEEKSRLLHCVVIGGGPTGVEFSGELSDFITRDVRQRYSH 319
            **********************************  ***  ***** ********************** **********
                                              +- + + +  +    -  +

SrNDA1  317 VKDYVRVTLIEANEILSSFDVSLRQYATNHLQKSGVRLVRGVVKEVLPKKIILNDGTDVPYGLLVWSTGVGASGFIKSLN 396
SrNDA2  317 VKDYVRVTLIEANEILSSFDVGLRQYATNHLQKSGVRLVRGVVKEVLPRKIILNDGTEVPYGLLVWSTGVGASGFIKSLN 396
AmNDA1  320 VKDYVRVTLIEANEILSSFDVSLRQYATNHLTKSGVRLVRGVVKEVMPKKILLSDGTEVPYGLLVWSTGVGPSGFTKSID 399
            ********************* *********  ************** * ** ** ** *************** *** **
                      + + +

SrNDA1  397 LPKSPGGRIGIDEWMRVPSVEDVFALGDCAGFLEQTGRPVLPALAQVAEREGKYLAELFVKIGKQDGGRAFSAKDASLGD 476
SrNDA2  397 LPKSPGGRIGIDEWLRVPSVEDVFALGDCAGFLEQTGRPVLPALAQVAEREGKYLAELFVKIGKQDGGRAFSAKDASLGD 476
AmNDA1  400 LPKSPGGRIGIDEWLRVPSVDDVFALGDCAGFLQETGKPVLPALAQVAERQGKYLADLLNRIGKQNGGKAFASRGIDLRD 479
            ************** ***** *********** * ** ************** ***** *    **** **  **   * *

SrNDA1  477 PFVYKHFGSMASVGGYKALVDLRQSKDAKGLTMAGFVSWFVWRSAYLTRVVSWRNRFYVATNWATTLVFGRDNSRIG    553
SrNDA2  477 PFVYKHFGSMASVGGYKALVDLRQSTDAKGPTLAGFGSWFIWRSAYLTRVVSWRNRFYVAANWATTLVFGRDNSRIG    553
AmNDA1  480 PFVYRHLGSMASVGRYKALVDLRQSKDAKGLAMAGFVSWFIWRSAYLTRVVSWRNRFYVAVNWATTLVFGRDNSRIG    556
            ****  * ****** *********** ****   *** **** ****************** *****************
```

Figure S1   Deduced amino acid sequences of SrNDA1, SrNDA2 and AmNDA1

Sequence alignments of SrNDA1, SrNDA2 and AmNDA1 were generated by GENETYX version 6.1. Underlined regions are mitochondrial targeting sequences predicted by Mitoprot. Asterisks indicate conserved amino acid residues among the three NDA sequences. Both the + and − signs under the alignments represent putative positions for two dinucleotide-fold fingerprints. Consistency of the respective positions in terms of these motifs is denoted by the different symbols: +, consistent; −, inconsistent.

---

[1]   To whom correspondence should be addressed (email kikuito@iwate-u.ac.jp).

```
SrNDB1    1 MRFTGASSTIY----QAVRRNSAFSKLLVVFAVGSGGLVVYADANPNHGLITEQSEVSAKKKVVVLGTGWAGTSFLKNLD  76
SrNDB2    1 MRFTGASSTIY----QAVRRNSAFSKLLVVFAVGSGGLVVYADAKPNHSLITEQSEVPAKKKVVVLGTGWAGTSFLKNMD  76
AmNDB1    1 MPPTS---GFFDLASGLLRRNPGFSRLLVVFAVGGGGLVVYADSNADLGVPSEQNKMPTKKKVVILGTGWAGTSFLKNLD  77
            *  *         ***  ** ******** *******         **        ***** ************* *
                                                           ++ + + +  +   +   +

SrNDB1   77 SSLYDVQVVSPRNYFAFTPLLPSVTCGTVDARSVVEPIRKIIKKKGGEIKFWEAECYNIDPGNKKVHCRSNIGTNLEGNG  156
SrNDB2   77 SSLYDVQVVSPRNYFAFTPLLPSVTCGTVDARSVVEPIRKIIKKKGGEIRFWEAECYNVDPVNKKVHCRSNIGTNLEGNG  156
AmNDB1   78 SSLYDVHVVSPRNYFAFTPLLPSVTCGTVDARSIVEPVRNIIRKKGGGVKFWEADCCKIDPTTKKVCRSNVGTNLEGNG  157
            ****** ************************** *** * ** ****    **** *   **  *** **** ********
                       + + -

SrNDB1  157 EFVVEYDYLVVTLGAKANTFNTPGVVEHCHFLKEVEDALRIRRSVMDCFERASLPNLTDEERKTNLHFIIVGGGPTGVEF  236
SrNDB2  157 EFVVEYDYLVVALGAKANTFNTPGVVEHCHFLKEVEDALRIRRSVMDCFERASLPNLTDEERKTNLHFIIVGGGPTGVEF  236
AmNDB1  158 EFVVDYDYLVVAIGARANTFNTPGVTENCHFLKEVEDAQRIRRSVIDCFERASLPTLSDEERKKNLHFVIVGGGPTGVEF  237
            **** ****** ** ********* * *********** ****** ********* * ***** **** ***********
                                                                ++ + + +  +

SrNDB1  237 AAELHDFVSEDIAKLYPRVRDLVKISVIEAGEHILTMFDKRITAFAEEKFKRDGIDVKTGYRVVKVSDKEIIMTGKATGE  316
SrNDB2  237 AAELHDFVSEDIAKLYPRVRDLVKISVIEAGEHILTMFDKRITAFAEEKFKREGIDVKTGYRVVKVSDKDIIMTGKATGE  316
AmNDB1  238 AAELHDFVNEDLSKLYPKVQELVKISVIEAGEHILTMFDKRITEFAEGKFQREGIDVKTGYKVVKVSDKSISMVSKEAGE  317
            ******** ** ****  *  ****************** *** ** * ********* ****** *  *   **
                 +  +           + + +

SrNDB1  317 TAVPYGMAVWSTGIGTRPVILDFMKQIGQVDRRVLATDEWLRVRGCDGVYALGDCATISQRKVMDDISAIFKVADKDNSG  396
SrNDB2  317 IAIPYGMAVWSTGIGTRPVILDFMKQIGQADRRVLATDEWLRVRGCDGVYALGDCATISQRKVMDDISAIFKVADKDNSG  396
AmNDB1  318 IDVPYGMAVWSTGIGTRPVILDFMKQIGQGDRRVLATDEWLRVRGCDGVYALGDCATITQRRVMDDISSIFRVADKDNSG  397
              ****************************** ***************************** ** ****** ** ********
                                                                           # # ##

SrNDB1  397 TLTVKEIQDVLGDICERYPQVELYLKSKQMEDFVDLLEDSKGNAKKESIELDIEQFKKALAHVDFQVKNLPATAQVAAQQ  476
SrNDB2  397 TLTVKEIQDVLGDICERYPQVELYLKSKQMEDFVDLLEDSKGNAKKESIELDIEQFKKALAHVDFQVKNLPATAQVAAQQ  476
AmNDB1  398 TLTVKEINDVLGDICERYPQVELYLKSKQMKSLVDLLKESEGNAKKETMELNIEQFKKALENVDSQVKNLPATAQVASQQ  477
            ******* **********************    **** * ****** ** ********  ** ************ **
                       ##   ##

SrNDB1  477 GYYLARCFNVMKNVEENPEGPLRMRESGRHRFRPFRYKHLGQFAPLGGEQTAAQLPGDWISIGYGSQWLWYSVYASKQVS  556
SrNDB2  477 GYYLARCFNVMKNVEENPEGPLRMRESGRHRFRPFRYKHLGQFAPLGGEQTAAQLPGDWISIGYGSQWLWYSVYASKQVS  556
AmNDB1  478 GAYLARCFNLLQNIDVNPEGPIRIRESGRHRFRPFRYRHLGQFAPLGGEQTAAQLPGDWISIGYGSQWLWYSVYASKQVS  557
            * *******   *      ***** * ************* ****************************************

SrNDB1  557 WRTRLSVVSDWTRRFIFGRDSSCI                                                          580
SrNDB2  557 WRTRLSVVSDWTRRFIFGRDSSCI                                                          580
AmNDB1  558 WRTRVAVVSNWTRRFIFGRDSSSL                                                          581
            ****  *** ************
```

Figure S2   Deduced amino acid sequences of SrNDB1, SrNDB2 and AmNDB1

Sequence alignments of SrNDB1, SrNDB2 and AmNDB1 shown in the same manner as described in Figure S1. In addition, # under the alignments indicates the putative positions for a Ca^{2+}-binding EF-hand motif.
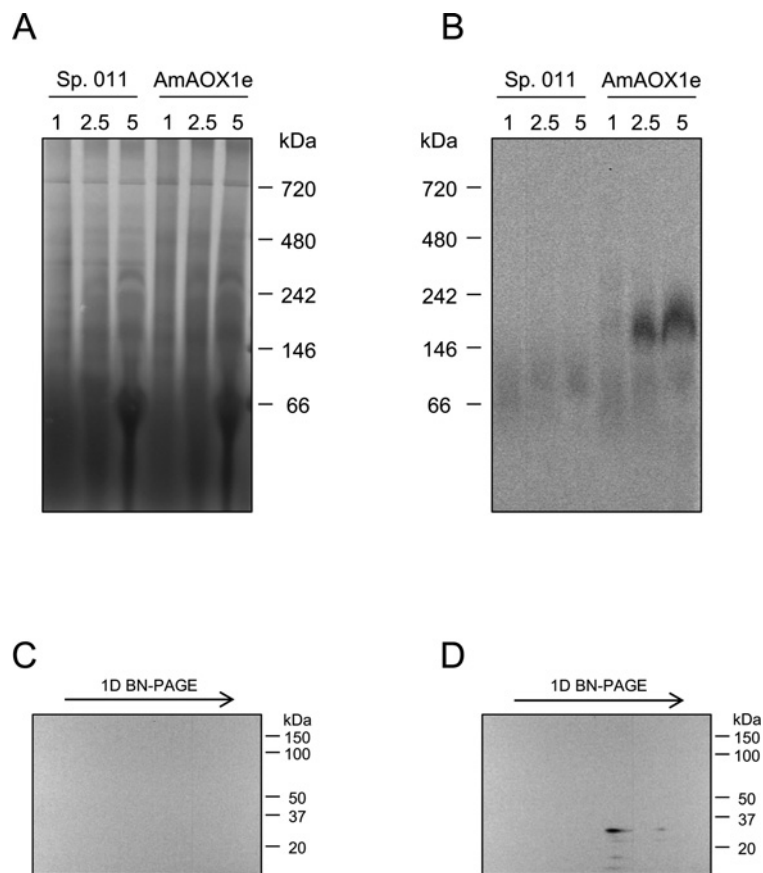
Figure S3 Immunological identification of AOX in *S. renifolius* mitochondria following 1D BN-PAGE under a range of experimental conditions

(**A**) *S. renifolius* mitochondria, which had experienced two freeze–thaw cycles, were solubilized using four different concentrations of digitonin, namely 1, 2.5, 5 and 10 g/g of protein, and were then resolved on to a 1D BN-PAGE gel. AOX was immunologically detected as shown in Figure 4(A) of the main text. The numbers above each lane indicate the digitonin concentrations. The molecular masses of standard proteins are indicated to the right-hand side of the image in kDa. The third lane from the left end is identical to the SR lane in Figure 4(A) of the main text. (**B**) Freshly-prepared *S. renifolius* mitochondria which had undergone no freeze–thaw cycles were solubilized using 5 g digitonin/g of protein, and were then run on a 1D BN-PAGE gel. AOX was immunologically detected as shown in Figure 4(A) of the main text. In the right image as a comparison, AOX was detected in mitochondria that had undergone two freeze–thaw cycles, which is identical to the SR lane in Figure 4(A) of the main text. The molecular masses of the standard proteins are shown between the two images in kDa. FP, freshly-prepared mitochondria; FT, mitochondria that had undergone two freeze–thaw cycles.

Figure S4   Immunological identification of AOX in mitochondria from non-transformed _S. pombe_ and its transformant expressing AmAOX1e

Mitochondria that had undergone two freeze–thaw cycles were solubilized by digitonin and were subjected to Western blotting after either 1D BN-PAGE or 2D BN/SDS/PAGE. (**A**) The proteins were stained by Coomassie Brilliant Blue after 1D BN-PAGE to show their appropriate loading and separation. (**B**) Immunological detection of AOX after 1D BN-PAGE. Numbers above each lane represent digitonin concentrations in g/g of protein. (**C**) Immunological detection of AOX in mitochondria from the non-transformed yeast after 2D BN/SDS-PAGE. The mitochondria were solubilized using 5 g of digitonin/g of protein. The result is presented as in Figure 4(B) of the main text. (**D**) Immunological detection of AOX in mitochondria from the transformant after 2D BN/SDS/PAGE. The results were shown in the same manner as in (**C**).

Table S1   DNA sequences of the primers used for RT–PCR and real-time PCR

Name	Sequence (5′→3′)
NDAF1	AACCACATGGTNTTCAC
NDAF2	CAYGCTCAAGAAATAAGGAA
NDAF3	ATCTTCCTCCGCGAGGT
NDAR1	ACAGTWGCCATGCTTCC
NDAR2	CTTTCTGCAACCTGAGC
NDAR3	ACCTGTTCCTCCAGCTCAC
NDBF1	AAGGAAGTAGAGGATGCTCA
NDBF2	ACTGGWGTGGARTTTGC
NDBF3	CTGCWGAGCTTCATGAYT
NDBF4	CATGTTTGACAARAGAATYAC
NDBR1	GCRACCTGAGCTGTTGC
NDBR2	ACTTGYTTGCTKGCATA
NDBR3	CCTCCCARTGGAGCAAA
NDBR4	ATRTCTTCCATGACTTTGCG
EF1aF1	ACATTGTGGTCATTGGCCA
EF1aR1	ACCAGTTGGGTCCTTCTT
SrNDAF1	GTGAAGGATTACGTACGAGTTACCC
SrNDAF2	GATTACACAAGTGTTCGGCGTC
SrNDAR1	GGGTAACTCGTACGTAATCCTTCAC
SrNDAR2	CGTACAACAACTCATCAAGACACC
SrNDBF1	GGTATGGCTGTCTGGTCTACTGG
SrNDBF2	GTGATGGTGTGTATGCACTTGG
SrNDBF3	ATCTCCATTTCTGCTGTGGTTC
SrNDBR1	CCAAGTGCATACACACCATCAC
SrNDBR2	CCAGTAGACCAGACAGCCATACC
SrNDBR3	CAAGCATTCTGCAATTAGCAGC
AmNDAF1	GTAAAGGATTACGTTCGCGTGAC
AmNDAF2	GAACAAAGCGAGAAATTGACCTC
AmNDAF3	TGCGTTCTAGTGCCCTCCTC
AmNDAR1	GTCACGCGAACGTAATCCTTTAC
AmNDAR2	TTCCACACATCTGCAGTCTCC
AmNDAR3	TGTAACTAGTATCTGGTAGGTTTCTGC
AmNDBF1	GAATGGCTGTCTGGTCTACTGG
AmNDBF2	AGAATCTCTAGAGGGAACGCTTGG
AmNDBR1	CCAAGTGCATAAACCCCATCAC
AmNDBR2	ACCTGGGATTTTCGGTGATG
AmSrEF1aF1	CGTCAAGTTTGCCGAGATCC
AmSrEF1aR1	GCTCAGCCTTCAGCTTGTCAAG
AmSrEF1aR2	CTCTTGTTCATCTCAGCAGCTTC
SrEF1aF1	ACATGGGGCTCTTCAGCA
SrEF1aR1	CCACTCATTATAACTAGTCAACATGCG
AmEF1aF1	ACGGCCAATCTCTGGATC
AmEF1aR1	GGAACGGTGGACAAGGAG
rtNDAF1	GACTGTGCAGGTTTTCT
rtNDAR1	TAGAACCTGTTCCTCCAGC
rtNDBF1	CATATTTTGACCATGTTTGA
rtNDBR1	CAGTAGACCAGACAGCCAT
rtEF1aF1	AGCATTGTGGTCATTGG
rtEF1aR1	CTCTTGTTCATCTCAGCAG